Nanoscale

PAPER

View Article Online
View Journal | View Issue

Cite this: *Nanoscale*, 2018, **10**, 18186

Arrays of highly complex noble metal nanostructures using nanoimprint lithography in combination with liquid-phase epitaxy†

Eredzhep Menumerov,‡[a] Spencer D. Golze,‡[a] Robert A. Hughes [a] and Svetlana Neretina *[a,b]

Current best-practice lithographic techniques are unable to meet the functional requirements needed to enable on-chip plasmonic devices capable of fully exploiting nanostructure properties reliant on a tailored nanostructure size, composition, architecture, crystallinity, and placement. As a consequence, numerous nanofabrication methods have emerged that address various weaknesses, but none have, as of yet, demonstrated a large-area processing route capable of defining organized surfaces of nanostructures with the architectural diversity and complexity that is routinely displayed in colloidal syntheses. Here, a hybrid fabrication strategy is demonstrated in which nanoimprint lithography is combined with templated dewetting and liquid-phase syntheses that is able to realize periodic arrays of complex noble metal nanostructures over square centimeter areas. The process is inexpensive, can be carried out on a benchtop, and requires modest levels of instrumentation. Demonstrated are three fabrication schemes yielding arrays of core–shell, core–void–shell, and core–void–nanoframe structures using liquid-phase syntheses involving heteroepitaxial deposition, galvanic replacement, and dealloying. With the field of nanotechnology being increasingly reliant on the engineering of desirable physicochemical responses through architectural control, the fabrication strategy provides a platform for advancing devices reliant on addressable arrays or the collective response from an ensemble of identical nanostructures.

Received 24th August 2018,
Accepted 19th September 2018

DOI: 10.1039/c8nr06874g

rsc.li/nanoscale

1. Introduction

The integration of nanomaterials with wafer-based fabrication techniques remains one of the fundamental challenges in advancing devices reliant on the remarkable properties accessible when materials are reduced to the nanoscale.[1] Substrate immobilized noble metal nanostructures are particularly compelling in this regard since functionality is derived from a range of properties that include plasmonic resonances, intense near-fields, hot electron generation, plasmonic heating, refractive index sensitivity, and catalytic activity. Their potential impact is further amplified when (i) formed in addressable arrays that allow for the interrogation of individual structures with optical, electrical, or scanning microscopy probes, (ii) arranged in patterns that promote a coupled response between adjacent nano- and bulk-scale materials, (iii) integrated with biopatterns, (iv) functionalized with analyte receptors, (v) incorporated into circuitry, or (v) integrated into microfluidic or lab-on-a-chip platforms. Collectively, such capabilities have the potential to revolutionize a diverse range of applications with a scope that includes biological and chemical detection,[2] photovoltaics,[3] metasurfaces,[4] and even nanofabrication itself.[5] Capitalizing on these opportunities is, however, reliant on the establishment of a processing science that is currently challenged by the often stringent demands that these applications place on nanostructure size, composition, architecture, crystallinity, and placement. Advancing methodologies that address these demands are, hence, of critical importance.

Electron-beam lithography is the most widely used technique for defining organized patterns of substrate-based noble metal structures with nanometer-scale dimensions. The advantages of this top-down technique include ultrahigh resolution, the accurate positioning of structures, high fidelity, and ease of integration into solid-state device fabrication. At the same time, it suffers from numerous deficiencies that include (i) a technically demanding serial writing process that is cost-prohi-

[a]*College of Engineering, University of Notre Dame, Notre Dame, Indiana, 46556, USA. E-mail: sneretina@nd.edu*
[b]*Department of Chemistry and Biochemistry, University of Notre Dame, Notre Dame, Indiana, 46556, USA*

†Electronic supplementary information (ESI) available: Description of the nanoimprint lithography system and additional characterization of the nanostructures. See DOI: 10.1039/c8nr06874g

‡Equal contribution.

bitive, time-consuming, and often impractical when forming nanostructures over square centimeter areas, (ii) a resolution that is challenged to define nanogaps between plasmonic nanostructures that maximize the intensity of hot spots, (iii) the use of adhesion layers that severely damp plasmonic resonances,[6] and (iv) an inability to define three-dimensional multi-element structures with the crystallinity and architectural diversity that is now routinely demonstrated using colloidal syntheses. Attempts to mitigate these deficiencies have relied on increasingly complex e-beam instrumentation and procedures[7] as well as post-processing of the lithographically-defined structures so as to promote crystallinity[8] and alloying.[1a,9] The so-formed structures are, however, still comparatively simple when compared to their colloidal counterparts.

With e-beam lithography having its shortcomings, numerous methods and innovative concepts have emerged that overcome many of its deficiencies. Nanoimprint lithography (NIL), which is of specific relevance to the current study, has emerged as an attractive process for forming periodic arrays with nanoscale features over large areas with a high throughput.[10] In this process, a lithographically-defined stamp is used to imprint a pattern into a moldable polymeric resist. Even though the stamp itself is made using e-beam lithography, its commercial availability and reusability make NIL a relatively low-cost and technologically straightforward benchtop process. The metal patterns produced can also undergo post-processing procedures such as templated dewetting[1a] to obtain crystalline structures with even smaller dimensions.[11] Other low-cost methods for forming periodic arrays of metal nanostructures involve the use of lithographically-defined shadow masks[12] or self-assembled surfaces formed using colloids,[13] anodized aluminum oxide (AAO),[14] or diblock copolymers.[15] Shadow masks with nanoscale openings, however, have limited reusability while self-assembled surfaces are typically limited by the number of patterns accessible and defects that disrupt long-range order. The Mirkin group has forwarded an alternative approach for forming metal nanoparticle arrays that uses arrays of scanning probes to site-selectively deposit attoliter droplets containing chemical precursors that when heated each form a single metal nanostructure.[16] While all of the aforementioned techniques have advanced array fabrication, the structures formed remain relatively simple in terms of architecture and composition. While such structures unquestionably have numerous functionalities, they are somewhat at odds with the field of nanotechnology that is, to a large degree, driven by engineering desirable physicochemical responses through architectural control.

With solution-based chemistry providing the only means to engineer a library of complex nanostructure geometries, a number of hybrid strategies have emerged where lithographically-defined features are used to regulate the placement of colloidal nanostructures. These techniques, which fall under headings such as capillary assembly,[1,17] template guided assembly,[18] chemical contrast patterning,[19] and DNA-mediated assembly,[20] have all proven effective in the site-selective placement of colloidal nanostructures. While unquestionably impressive, the downside of these techniques include a yield that is limited by the homogeneity of the colloid, target sites that are fabricated using e-beam lithography, and challenges associated with the alignment of asymmetric structures. An alternate approach, which has been advanced by our group, uses solid-state dewetting to form architecturally simple nanostructures that are then transformed into complex nanostructures using liquid-phase chemistry.[21] This work, along with the work of other groups[22] who have carried out variations to this approach, have collectively fabricated the most sophisticated substrate-based nanostructures produced to date. These demonstrations have, however, yielded either randomly distributed structures or periodic arrays over small areas. Here, we demonstrate a hybrid nanofabrication scheme for forming nanostructured arrays of highly complex nanostructures over a square centimeter area through the integration of NIL, directed-assembly, and solution-based growth modes. The method advances the goal of fabricating organized surfaces of engineered nanostructures in a manner that is responsive to scalability, throughput, and cost-effectiveness.

2. Results

2.1. Fabrication strategy

The strategy used to fabricate periodic arrays of complex metal nanostructures relies upon a three-stage processing route. The first stage utilizes NIL as a means to impose a periodicity over the substrate surface by creating an array of openings through a deposited resist that act as target sites for the formation of metal nanoparticles. The second stage sees the deposition of the metal through the openings, the removal of the resist, and a heat treatment that results in the agglomeration and crystallization of the metal at the center of each target site. In the final stage, the substrate-immobilized nanoparticles are subjected to wet-chemistry protocols in which each particle seeds an identical reaction whose product is a nanostructure of increased sophistication. In the ensuing sections, we demonstrate this nanofabrication route by forming periodic arrays of Au seeds using NIL and then transform them into progressively more intricate nanostructures using three different solution-based protocols.

2.2. Seed fabrication

The processing route used to fabricate periodic arrays of Au seeds is shown schematically in Fig. 1a. A moldable polymeric resist is spin-coated onto a planar (0001)-oriented sapphire substrate and baked. The resist is then embossed with a 1 cm^2 silicon stamp consisting of a periodic array of pillars (diameter = 275 nm, height = 350 nm) arranged in a square pattern (pitch = 580 nm), a procedure carried out at elevated temperatures and pressures using a commercially available stamp in combination with a home-built pneumatic nanoimprinting press (see ESI, Fig. S1†). At this stage, the bottom of each cylindrical hole does not reach the substrate surface as denoted by the red arrow in Fig. 1b. Openings to the surface are made by exposing the

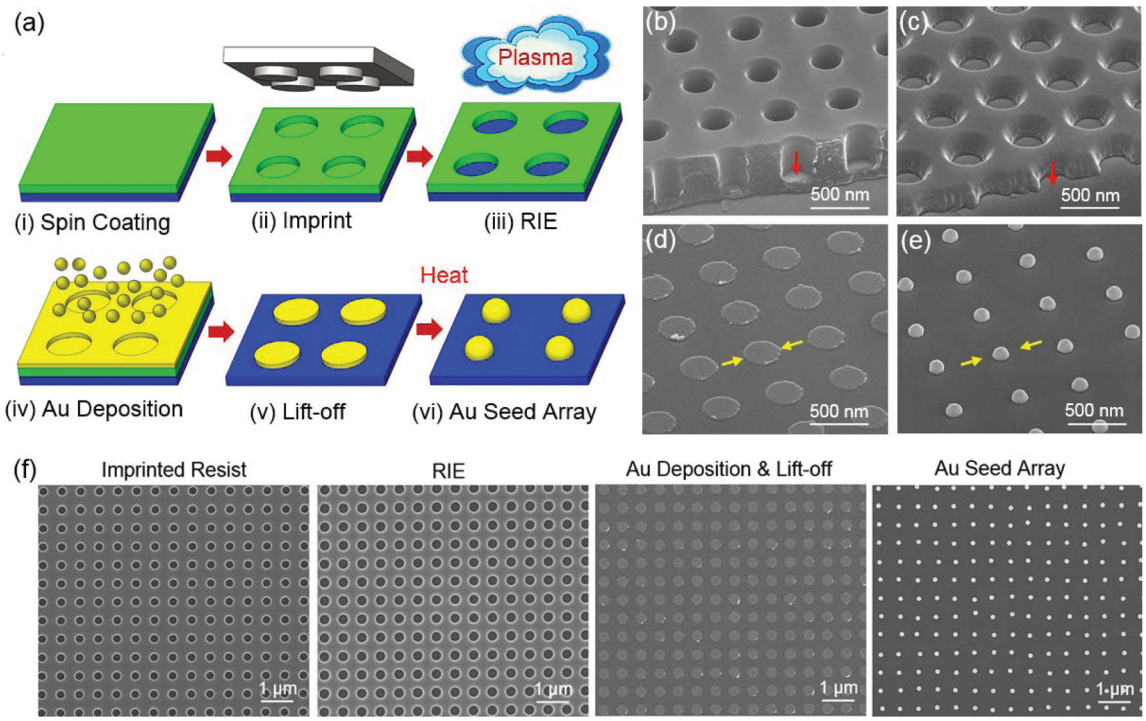

Fig. 1 (a) Schematic of the six step procedure used to form periodic arrays of Au nanostructures using NIL followed by templated dewetting. Tilt-view SEM images of the (b) imprinted resist, (c) the imprinted resist after being exposed to an RIE treatment, (d) polycrystalline Au discs formed through deposition and lift-off, and (e) crystalline Au seeds. Note that a scratch was made in the resist to expose the edges seen in (b) and (c). (f) Top-view SEM images of the same process over larger areas.

resist to a reactive ion etch (RIE) (Fig. 1c) that gradually thins the resist while leaving any exposed substrate intact (*i.e.*, the substrate remains planar). Room temperature physical vapor deposition is then used to deposit an 18 nm thick layer of Au into the openings and onto the remaining resist. Films produced in this manner are polycrystalline with nanometer-scale grains.[23] A lift-off procedure is then carried out to dissolve the resist and remove the Au deposited on its surface, a process that leaves behind an array of circular Au discs on the substrate (Fig. 1d). When heated, the discs undergo a dewetting process that sees them transformed into weakly faceted structures with a near-hemispherical geometry (Fig. 1e) of smaller diameter than the initial Au disc (yellow arrows in Fig. 1d and e). It is these structures that act as seeds for solution-based growth modes. Fig. 1f shows top-view SEM images of the same process over larger areas.

Forming periodic arrays of nanostructures using NIL in combination with templated dewetting, like any nanofabrication technique, has both advantages and limitations. Its foremost advantage is that it provides a large-area capability (see ESI, Fig. S2†). The NIL stamp used to produce the array in Fig. 1e, for example, results in the formation of 2×10^8 Au nanostructures over a centimeter-square substrate. In addition, it is a relatively straightforward process, requires only modest levels of instrumentation, can be carried out on a benchtop in few hours, and does not require clean-room facilities. The NIL stamps do, however, ultimately limit the density at which structures can be produced and show damage over time that leads to arrays with missing structures (see ESI, Fig. S3†). The use of templated dewetting not only results in the formation of crystalline structures but also presents the opportunity to crystallographically align the structures if a heteroepitaxial relationship is formed with the substrate.[21b] Substrates that are likely amenable to Au heteroepitaxy are [0001]-oriented surfaces with a hexagonal crystal structure or [111]-oriented surfaces with a cubic structure. The substrate must also have a low surface energy relative to Au, should be able to withstand the processing temperatures needed for dewetting, and should not allow Au to interdiffuse. Having a well-defined number of Au atoms deposited in each of the openings in the resist leads to a high degree of size uniformity (see ESI, Fig. S4†). While it is possible to vary the size of the structure by adjusting the amount of Au deposited, there are limits on the degree to which this can be done. If the thickness of the lithographically-defined Au disk is too thin, then it gives rise to instabilities in the dewetting process that cause the Au disc to break up into multiple islands at each array site (see ESI, Fig. S5†). At this point, arrayed structures with a smaller diameter can only be formed through the use of a stamp with smaller feature sizes or the use of a modified assembly process that accelerates dewetting through the incorporation of a sacrificial Sb layer.[24] The templated dewetting process is also imperfect in that it leads to variability in the nanostructure center-to-center distances (see ESI, Fig. S4†). Asserting control over the nano-

structure shape is also difficult because the high temperatures used in the dewetting process drive the nanostructure geometry toward that which is thermodynamically favorable, where little can be done to alter it.[25]

2.3. Solution-based growth modes

Once fabricated, the Au seed arrays were subjected to solution-based syntheses adapted from one of the many seed-mediated protocols that have been devised to generate colloidal nanostructures. Each of the three examples presented herein were carried out in aqueous solutions heated to 95 °C using only a beaker and hot plate. While such syntheses require little in the way of instrumentation, architectural control is afforded by the chemical environment in which the seeds are immersed. With the use of Au seeds that are well-bound to the substrate comes the added advantage that they can be transferred from one chemical environment to another in rapid succession, a capability that is unavailable to colloidal growth modes. In this section, such chemical controls are used to transform Au seed arrays into core–shell, core–void–nanoshell, and core–void–nanoframe nanostructures.

2.3.1. Arrays of core–shell structures. The synthesis, characterization, and application of colloidal bimetallic nanostructures has demonstrated a versatility and utility that greatly exceeds their monometallic counterparts.[26] Such structures derive benefit from the greater range of physicochemical properties accessible when two metals form a nanoscale interface or are combined to obtain an alloy or intermetallic compound. One of the most fundamental bimetallic architectures is the core–shell structure (abbreviated as core@shell) in which one metal is heterogeneously deposited on a second metal. Such syntheses can lead to growth modes that promote specific facets and where the two metals form a heteroepitaxial relationship with each other. Such reactions typically proceed by adding metal seeds and a reducing agent to an aqueous solution of metal ions of a second metal. The ensuing reaction sees the ions transformed into a neutral species that readily deposits on the seed material (*e.g.*, Ag^+ being reduced to Ag). Fig. 2 shows a schematic representation of the shape transformation, SEM images, and elemental mapping of a periodic array of Au@Ag core–shell structures obtained when carrying out a liquid-phase synthesis in which Ag^+ ions, derived from $AgNO_3$, are reduced onto Au seeds by ascorbic acid. The product of the reaction is a highly faceted structure that expresses square (100) and hexagonal (111) Ag facets. This facet pattern, along with the fact that the structures show in-plane alignment with each other (Fig. 2c), reveal that the underlying Au seed is [111]-oriented and has a heteroepitaxial relationship with the substrate. Also noteworthy is that the so-formed core–shell structure is fundamentally different from its colloidal counterpart in that the shell does not completely encapsulate the core since the substrate prevents the growth solution from coming into contact with the underside of the Au seed. Nonetheless, the ability to fundamentally transform the Au seed array in a reaction lasting 12 min demonstrates the potency of this wet-chemistry approach.

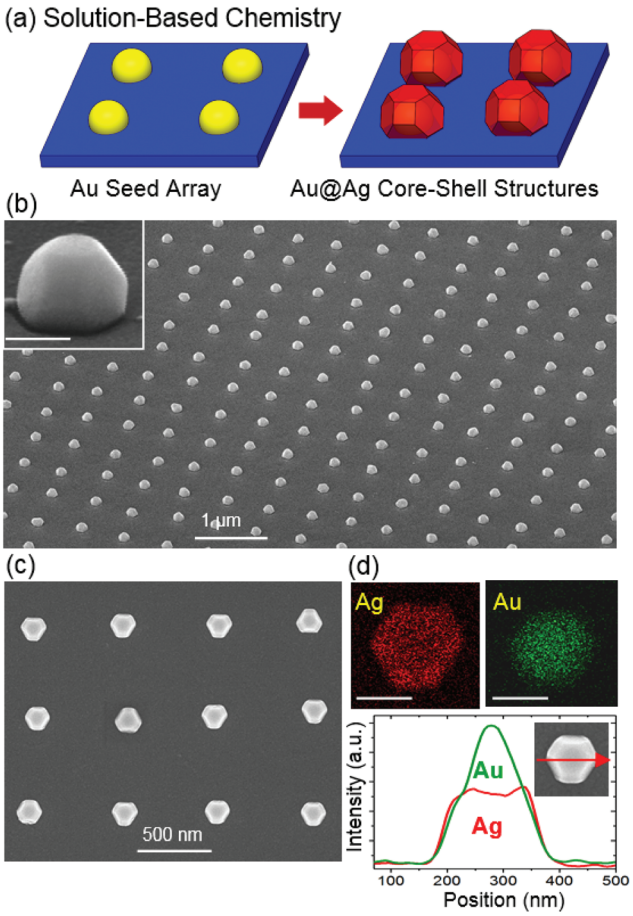

Fig. 2 (a) Schematic showing the transformation that occurs when Au seeds are transformed into faceted Au@Ag core–shell structures using solution-based chemistry. SEM images of the Au@Ag structures taken from a (b) tilted- and (c) top-view. (d) EDS maps and line scans of an individual core–shell structure (scale bar = 100 nm).

2.3.2. Arrays of core–void–shell structures. Some of the most sophisticated nanostructures have emerged from reactions that incorporate chemistries that hollow part of an existing structure through the use of a preferential etch, the Kirkendall effect, or galvanic replacement reactions.[27] Associated with this complexity are properties that continuously change as the structure advances through a hollowing process that alters both the morphology and composition and which can be halted at any intermediate point in the reaction. Galvanic replacement reactions are particularly intriguing in this regard in that hollowing is accompanied by the deposition of a secondary metal. Such reactions occur spontaneously when a solid metal, often referred to as the template, is exposed to ions of a second metal with a higher electrochemical potential. The ensuing reaction sees the reduction and deposition of the aqueous metal onto the template as the solid metal template is oxidized to form ions that enter the liquid phase. The product of the reaction is typically a hollow shell with a composition that is an alloy of the two metals.

With each metal ion having its own distinct electrochemical potential, the hierarchy in these values becomes the deciding factor as to whether a galvanic replacement reaction can proceed. Au, being the noblest of metals, has the highest electrochemical potential and cannot be replaced by any metal ion. This renders the Au seeds immune to galvanic replacement reactions. If, however, Ag is first deposited on the Au seed to form an Au@Ag core–shell structure then the solid Ag shell can undergo replacement while leaving the Au core intact. Fig. 3a shows a schematic representation of a two-step liquid-phase synthesis where the Au seed is first transformed into an Au@Ag nanocube through the heterogeneous deposition of Ag and then further reconfigured into an Au@void@AgPd core–void–nanoshell through galvanic replacement. The first stage of the synthesis proceeds in much the same manner as in the previously described core–shell synthesis, but where a facet-selective capping agent acts to promote the formation of (100) facets. The product of the reaction, shown in Fig. 3b, is a [111]-oriented Au@Ag nanocube that is truncated on its underside by the substrate surface.

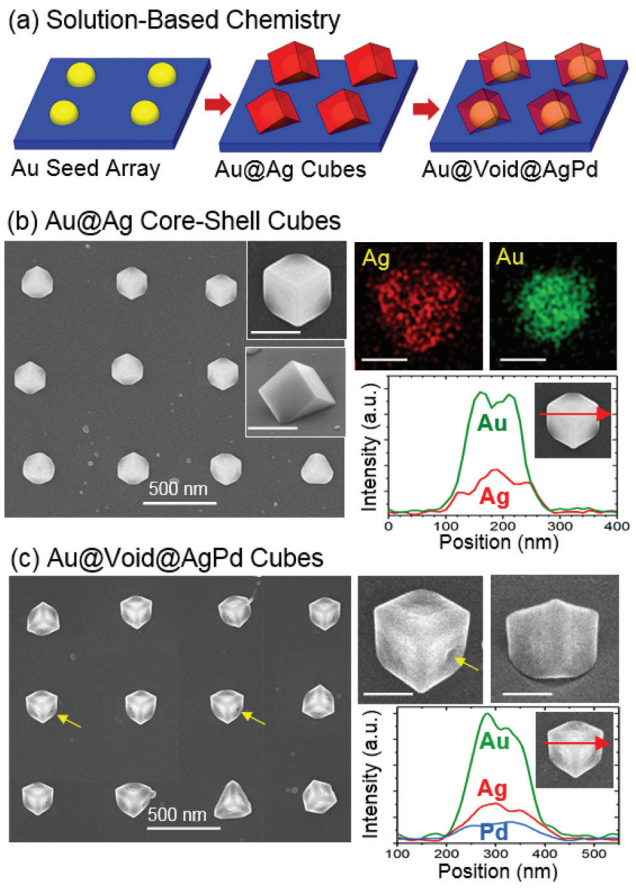

Fig. 3 (a) Schematic showing the transformation that occurs as Au seeds are first transformed into an Au@Ag core–shell nanocube and then into an Au@void@AgPd core–void–shell structure using a two-stage solution-based synthesis. Top-view SEM images and the associated elemental maps and line scans for the (b) Au@Ag and (c) Au@void@AgPd structures (scale bar = 100 nm).

These core–shell structures are then subjected to a galvanic replacement reaction where aqueous Pd^{2+} ions derived from Na_2PdCl_4 replace the Ag according to:

$$2Ag(s) + Pd^{2+}(aq) \rightarrow Pd(s) + 2Ag^{+}(aq).$$

With a two-to-one Ag–Pd replacement ratio, the reaction results in a significant volume loss. Fig. 3c shows an array of the so-formed Au@void@AgPd nanoshells and the associated EDS line scans. In these images the core becomes more visible due to the hollowing that has occurred. The cube geometry also becomes somewhat distorted in that its edges thicken relative to the sidewalls due to preferential deposition where the facets meet. The hole in the nanoshell through which the Ag^{+} ions exited the interior of the structure into the adjacent solution is clearly visible on several of the structures as is denoted by the yellow arrows. Such structures are unique to substrate-based syntheses since both the core and the shell are immobilized by bonds made to the substrate, whereas the analogous colloidal synthesis would result in a nanorattle structure[28] where the central core is free to move within the confining shell.

2.3.3. Arrays of core–void–nanoframe structures. In the previous synthesis the galvanic replacement reaction was terminated immediately after the supply of pure Ag was exhausted through the opening in the AgPd shell. If, however, the reaction is allowed to proceed, then it enters a dealloying phase where the Ag remaining in the alloy shell is replaced, a process that is relatively slow since it is only through solid state diffusion that the alloyed Ag is able to migrate to the nanoshell surface and enter the solution phase. As this occurs the shell composition trends toward that of a single element where shell volume is lost due to the non-unity replacement ratio. In such a scenario, the shell can undergo a morphological reconstruction that sees the sidewalls thin and collapse, leaving behind a frame-like structure. The colloidal synthesis and application of these so-called nanoframes have been widely studied and are the subject of two recent reviews.[29]

In a third demonstration of solution-based chemistry performed on arrayed Au seeds, Au@Ag core–shell nanocubes were prepared in a manner identical to those shown in Fig. 3b and then subjected to a galvanic replacement reaction that was allowed to continue through a dealloying phase. The reaction carried out saw aqueous Au^{3+} ions, derived from $HAuCl_4$, replace the solid Ag shell according to:

$$3Ag(s) + Au^{3+}(aq) \rightarrow Au(s) + 3Ag^{+}(aq).$$

Fig. 4 shows a schematic of the two-stage synthesis as well as SEM images and elemental mapping of the structures formed. The images reveal Au seeds confined within a framework that traces out the seams where the (100) facets of the Ag nanocube once met. EDS line scans indicate that the dealloying process has rendered the shell almost completely devoid of Ag (Fig. 4c). The structures are, once again, unique from their colloidal counterparts in that both the frame and core are rendered immobile by the substrate. With nanoscale gaps occurring between the outer framework and centralized core

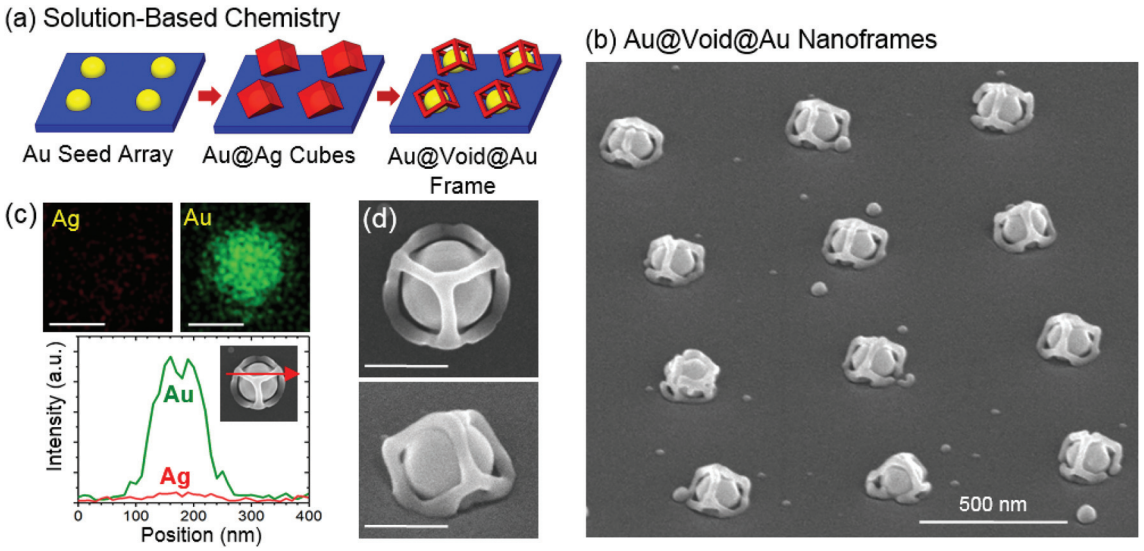

Fig. 4 (a) Schematic showing the two stage synthesis that first transforms Au seeds into an Au@Ag core–shell nanocube and then into an Au@void@Au core–void–nanoframe. (b) Tilted-view SEM image of the framed structures formed in a periodic array. (c) Elemental maps and EDS line scans showing that nearly all of the Ag has been removed from the final structure and (d) top- and tilted-view high magnification images of a single structure (scale bar = 100 nm).

(Fig. 4d), the synthesis has, in essence, transformed an autonomous nanostructure (*i.e.*, the Au@Ag nanocube) into two distinct structures. While this substrate-based synthesis gives rise to a greater structure-to-structure variation than the previous two syntheses (see ESI, Fig. S6†), the degree of architectural sophistication and control is unrivalled for noble metal nanostructures formed in periodic arrays.

3. Discussion

The incorporation of NIL into a nanofabrication strategy that is able to define truly complex metal nanostructures is significant in that periodic arrays can be formed over length-scales of relevance to device prototyping reliant on addressable arrays or the collective response from a set of identical nanostructures. Compared to our previous work,[24] which utilized TEM grids as shadow masks, NIL offers a more than 20-fold improvement in arrayed area and a 5-fold increase in nanostructure density. NIL also offers scalability, cost-effectiveness, a reasonable throughput, the ability to fabricate a wide selection of patterns using custom-made stamps, and is adaptable to metal–substrate combinations beyond that of the Au–sapphire example demonstrated here. When the NIL-defined patterns are exposed to a directed-assembly procedure followed by liquid-phase reactions, the resulting structures are far more complex than those derivable when using just NIL. This ability to generate such complex nanostructures originates from the numerous chemical controls available when carrying out solution-based chemistry and is amplified by a mature knowledge-base from which well-established colloidal syntheses can be obtained and then adapted to the substrate-based platform. As architectural control is gained, the ability to engineer the desired physicochemical properties is greatly expanded because changes to shape and composition allow for far greater tunability than does changes to the nanostructure size.

While the individual strengths of NIL, directed assembly, and liquid-phase epitaxy all contribute to this nanofabrication strategy, further advantage is derived through their integration. The immobilization of structures on a substrate, for example, allows for two-step liquid-phase syntheses where the emerging structures are rapidly transferred from one chemical environment to another by merely lifting the substrate out of one solution and placing it in another. Substrate-immobilization was also critical in the formation of the core–void–nanoshells and core–void–nanoframes because the nanogap is preserved through bonds formed to the substrate. The formation and control over such nanoscale gaps is one of the grand challenges facing nanofabrication due to the plasmonic hot spots that develop. Future opportunities also stem from the preparation of periodic arrays on substrate materials that not only support the nanostructures but then form a coupled optical, electronic, chemical, thermal, or magnetic response from which greater functionality is derived. While numerous colloidal growth modes are available for adaptation to substrate-based syntheses, there also exist opportunities in terms of using unconventional synthetic levers that are unique to substrate-based growth modes including: (i) a flow of reactants past an anchored substrate, (ii) synthetically-active substrate materials, (iii) substrate-imposed epitaxy, and (iv) lithographically-imposed barriers to growth. Together, these capabilities and opportunities provide for a platform that could markedly advance the nanofabrication and application of chip-based plasmonic devices.

4. Conclusion

This study provides a proof-of-concept for a nanofabrication strategy that effectively combines NIL, directed-assembly, and liquid-phase epitaxy to form periodic arrays of highly complex noble metal nanostructures over square centimeter areas using benchtop processing. By creating a platform in which nanostructures can be designed to express specific properties based on sophisticated architectures, the work could lead to the fabrication of chemically- and optically-active surfaces able to detect chemical and biological species, manipulate electromagnetic radiation, catalyze chemical reactions, or generate the hot electrons and intense plasmonic near-fields that activate photovoltaic devices.

5. Experimental section

5.1. Nanoimprint lithography

A moldable polymer resist (mr-I 7030R, Micro Resist Technology, GmbH) is spin-coated onto a 10 mm × 10.5 mm × 0.6 mm [0001]-oriented sapphire substrate that was diced from a 4 in. wafer (MTI). In this process, 4 drops of the resist (≈65 μL) are applied to a stationary substrate that is then spun to an initial speed of 500 rpm for 7 s to remove excess resist followed by 60 s duration spin at 1700 rpm to obtain a uniform coating with a thickness of 400 nm. The resist is then baked in air for 2 min on a hotplate set to 125 °C. Imprints made in the resist utilized a 1 cm^2 silicon nanopatterned stamp (Lightsmyth Technologies, patterned area 8 mm × 8.3 mm) to which a Trichloro(1*H*,1*H*,2*H*,2*H*-perfluoro-octyl) silane antisticking layer (Sigma Aldrich) was previously applied. The stamp pattern consists of a periodic array of 350 nm long, 275 nm diameter cylindrical pillars arranged in a square pattern with a 580 nm center-to-center distance. The stamp is placed in contact with the resist after which the combination is placed onto the preheated lower platen (140 °C) of a home-built pneumatic nanoimprinting press (see ESI, Fig. S1†). A pressure of 40 bar is then applied to the stamp surface by lowering the upper platen. After a 15 min duration the heating element is turned off and the resist is allowed to cool to a temperature below 50 °C. The stamp is then removed from the substrate and cleaned in acetone so that it is ready for reuse. The patterned resist is inserted into an RIE system that uses O_2 as the processing gas. Openings through the resist to the substrate surface are made by exposing the resist to a 90 s etch under an O_2 flow of 4 sccm and an RF power of 20 W.

5.2. Au film deposition and templated dewetting

Au films with a thickness of 18 nm were sputter deposited on the imprint to form a conformal layer over both the resist and exposed substrate. The film was deposited onto the rotating sample (30 rpm) at a rate of 13 nm min^{-1} using a beam energy of 6 keV, penning ion gun currents of 200 μA, and an Ar pressure of 7 × 10^{-5} Torr. Once removed from the sputter coater, the sample underwent a lift-off procedure in which the resist is dissolved in acetone while the Au that resided on its surface either peels away into the solution or is removed with an adhesive tape. The remaining patterned surface is rinsed in acetone and dried under a N_2 gas flow. The sample is placed in an alumina crucible and inserted into a quartz tube furnace with a flowing Ar atmosphere, heated to temperatures just above the Au melting point in 26 min, and then allowed to cool to room temperature.

5.3. Au@Ag core–shell synthesis

Au seeds were placed in 6 mL of aqueous $AgNO_3$ (1 mM) heated to 95 °C. The heterogeneous deposition of Ag onto the Au seed was then initiated by the addition of 2 mL of 95 °C aqueous ascorbic acid (10 mM) over a 2 min interval after which the reaction was allowed to proceed for an additional 10 min. The substrate was then removed from the liquid reactants, rinsed and sonicated for 30 s in DI water, and dried under flowing N_2. The sonication step removes structures from the substrate surface that resulted from unwanted spontaneous nucleation within the liquid medium.

5.4. Au@void@AgPd core–void–nanoshell synthesis

Au seeds are placed in an aqueous solution formed by combining 3 mL of 10 mM trisodium citrate ($Na_3C_6H_5O_7$) with 0.5 mL of 0.2 mM nitric acid (HNO_3) and heated to 95 °C. The heterogeneous deposition of Ag onto the seeds is initiated by rapidly adding 3 mL of aqueous $AgNO_3$ (1 mM, 95 °C), after which the reaction was allowed to proceed for 3.5 min. In this reaction, $AgNO_3$ is the source of Ag^+ ions, citrate acts as a reducing and provides the means by which (100) facets are capped,[21b] and HNO_3 inhibits the spontaneous nucleation of Ag colloids within the solution phase. Once the Au@Ag nanocubes are formed they are immediately transferred to a second solution of aqueous Na_2PdCl_4 (3 mL, 200 μM, 95 °C) in which a galvanic replacement reaction is allowed to proceed for 12 min. The replaced structures were rinsed in acetone and dried under an N_2 gas flow. Acetone is used instead of water in the rinsing step because the capillary forces occurring when water dries tend to damage the AgPd shells.

5.5. Au@void@Au core–void–nanoframe synthesis

Au@Ag nanocubes were synthesized using the procedure described in the previous synthesis. These core–shell structures were then immediately transferred to a second solution of aqueous $HAuCl_4$ (3 mL, 20 μM, 95 °C) where the galvanic replacement reaction was allowed to proceed for 12 min. The replaced structures were rinsed in acetone and dried under an N_2 gas flow.

5.6. Instrumentation

The NIL/templated dewetting process utilized a (i) Laurell Spin Coater, (ii) SAMCO RIE-1C Reactive Ion Etcher, (iii) Model 681 Gatan High Resolution Ion Beam Coater, and (iv) Lindberg Blue M quartz tube furnace. SEM images and the associated elemental analysis were obtained using a Magellan 400 FEI

Field Emission Scanning Electron Microscope (FESEM) equipped with Bruker XFlash Energy Dispersive X-ray detector.

Conflicts of interest

There are no conflicts to declare.

Acknowledgements

This work was supported by a National Science Foundation Award (CMMI-1707595) to S. N. The authors have benefited from the facilities available through the Notre Dame Integrated Imaging Facility (NDIIF). We also acknowledge B. Yuan and T. B. Demille for their assistance in the preparation of this manuscript.

Notes and references

1 (*a*) R. A. Hughes, E. Menumerov and S. Neretina, *Nanotechnology*, 2017, **28**, 282002; (*b*) S. Ni, L. Isa and H. Wolf, *Soft Matter*, 2018, **14**, 2978.

2 (*a*) W. Wang, *Chem. Soc. Rev.*, 2018, **47**, 2485; (*b*) T. Xie, C. Jing and Y. T. Long, *Analyst*, 2017, **142**, 409; (*c*) M. Li, S. K. Cushing and N. Wu, *Analyst*, 2015, **140**, 386; (*d*) S. Unser, I. Bruzas, J. He and L. Sagle, *Sensors*, 2015, **15**, 15684; (*e*) W. Li, L. Zhang, J. Zhou and H. Wu, *J. Mater. Chem. C*, 2015, **3**, 6479; (*f*) C. Wadell, S. Syrenova and C. Langhammer, *ACS Nano*, 2014, **8**, 11925; (*g*) K. M. Mayer and J. H. Hafner, *Chem. Rev.*, 2011, **111**, 3828; (*h*) J. N. Anker, W. P. Hall, O. Lyandres, N. C. Shah, J. Zhao and R. P. Van Duyne, *Nat. Mater.*, 2008, **7**, 442; (*i*) G. L. Liu, Y. T. Long, Y. Choi, T. Kang and L. P. Lee, *Nat. Methods*, 2007, **4**, 1015.

3 (*a*) K. Ueno, T. Oshikiri, Q. Sun, X. Shi and H. Misawa, *Chem. Rev.*, 2018, **118**, 2955; (*b*) P. Christopher and M. Moskovits, *Annu. Rev. Phys. Chem.*, 2017, **68**, 379; (*c*) A. Furube and S. Hashimoto, *NPG Asia Mater.*, 2017, **9**, e454.

4 (*a*) H.-H. Hsiao, C. H. Chu and D. P. Tsai, *Small Methods*, 2017, **1**, 1600064; (*b*) H. T. Chen, A. J. Taylor and N. Yu, *Rep. Prog. Phys.*, 2016, **79**, 076401.

5 (*a*) Z. Xie, W. Yu, T. Wang, H. Zhang, Y. Fu, H. Liu, F. Li, Z. Lu and Q. Sun, *Plasmonics*, 2011, **6**, 565; (*b*) J. M. Lee and B. Il Kim, *Mater. Sci. Eng. A*, 2007, **448–451**, 769.

6 T. Siegfried, Y. Ekinci, O. J. F. Martin and H. Sigg, *ACS Nano*, 2013, **7**, 2751.

7 (*a*) C. M. Soukoulis and M. Wegener, *Nat. Photonics*, 2011, **5**, 523; (*b*) J. Trasobares, F. Vaurette, M. François, H. Romijn, J. L. Codron, D. Vuillaume, D. Théron and N. Clément, *Beilstein J. Nanotechnol.*, 2014, **5**, 1918.

8 (*a*) K. Chennit, J. Trasobares, A. Anne, E. Cambril, A. Chovin, N. Clément and C. Demaille, *Anal. Chem.*, 2017, **89**, 11061; (*b*) N. A. Roberts, J. D. Fowlkes, K. Mahady, S. Afkhami, L. Kondic and P. D. Rack, *ACS Appl. Mater. Interfaces*, 2013, **5**, 4450.

9 F. A. A. Nugroho, B. Iandolo, J. B. Wagner and C. Langhammer, *ACS Nano*, 2016, **10**, 2871.

10 (*a*) L. J. Guo, *Adv. Mater.*, 2007, **19**, 495; (*b*) M. C. Traub, W. Longsine and V. N. Truskett, *Annu. Rev. Chem. Biomol. Eng.*, 2016, **7**, 583; (*c*) L. Gao, Y. Zhang, H. Zhang, S. Doshay, X. Xie, H. Luo, D. Shah, Y. Shi, S. Xu, H. Fang, J. A. Fan, P. Nordlander, Y. Huang and J. A. Rogers, *ACS Nano*, 2015, **9**, 5968; (*d*) M. Lee, J. U. Kim, K. J. Lee, S. Ahn, Y. B. Shin, J. Shin and C. B. Park, *ACS Nano*, 2015, **9**, 6206.

11 (*a*) H. Cai, H. Wolfenson, D. Depoil, M. L. Dustin, M. P. Sheetz and S. J. Wind, *ACS Nano*, 2016, **10**, 4173; (*b*) Z. Zhu, B. Bai, O. You, Q. Li and S. Fan, *Light: Sci. Appl.*, 2015, **4**, e296.

12 (*a*) K. D. Gilroy, P. Farzinpour, A. Sundar, T. Tan, R. A. Hughes and S. Neretina, *Nano Res.*, 2013, **6**, 418; (*b*) S. Aksu, A. A. Yanik, R. Adato, A. Artar, M. Huang and H. Altug, *Nano Lett.*, 2010, **10**, 2511.

13 (*a*) S. Kasani, P. Zheng and N. Wu, *J. Phys. Chem. C*, 2018, **122**, 13443; (*b*) A. Pravitasari, M. Negrito, K. Light, W. S. Chang, S. Link, M. Sheldon and J. D. Batteas, *J. Phys. Chem. B*, 2018, **122**, 730; (*c*) C. L. Haynes and R. P. Van Duyne, *J. Phys. Chem. B*, 2001, **105**, 5599; (*d*) H. Fredriksson, Y. Alaverdyan, A. Dmitriev, C. Langhammer, D. S. Sutherland, M. Zäch and B. Kasemo, *Adv. Mater.*, 2007, **19**, 4297; (*e*) V. Russo, N. Michieli, T. Cesca, C. Scian, D. Silvestri, M. Morpurgo and G. Mattei, *Nanoscale*, 2017, **9**, 10117; (*f*) S. Syrenova, C. Wadell and C. Langhammer, *Nano Lett.*, 2014, **14**, 2655; (*g*) C. M. Müller, F. C. F. Mornaghini and R. Spolenak, *Nanotechnology*, 2008, **19**, 485306.

14 (*a*) V. Fiehler, F. Patrovsky, L. Ortmann, S. Derenko, A. Hille and L. M. Eng, *J. Phys. Chem. C*, 2016, **120**, 12178; (*b*) Q. Hao, H. Huang, X. Fan, Y. Yin, J. Wang, W. Li, T. Qiu, L. Ma, P. K. Chu and O. G. Schmidt, *ACS Appl. Mater. Interfaces*, 2017, **9**, 36199; (*c*) H. Masuda and M. Satoh, *Jpn. J. Appl. Phys.*, 1996, **35**, L126.

15 (*a*) J. Y. Kim, H. Kim, B. H. Kim, T. Chang, J. Lim, H. M. Jin, J. H. Mun, Y. J. Choi, K. Chung, J. Shin, S. Fan and S. O. Kim, *Nat. Commun.*, 2016, **7**, 12911; (*b*) C. Garozzo, R. A. Puglisi, C. Bongiorno, S. Scalese, E. Rimini and S. Lombardo, *J. Mater. Res.*, 2011, **26**, 240; (*c*) C. M. Bates, M. J. Maher, D. W. Janes, C. J. Ellison and C. G. Willson, *Macromolecules*, 2014, **47**, 2.

16 (*a*) P. C. Chen, G. Liu, Y. Zhou, K. A. Brown, N. Chernyak, J. L. Hedrick, S. He, Z. Xie, Q. Y. Lin, V. P. Dravid, S. A. O'Neill-Slawecki and C. A. Mirkin, *J. Am. Chem. Soc.*, 2015, **137**, 9167; (*b*) P. C. Chen, X. Liu, J. L. Hedrick, Z. Xie, S. Wang, Q. Y. Lin, M. C. Hersam, V. P. Dravid and C. A. Mirkin, *Science*, 2016, **352**, 1565; (*c*) L. Chen, X. Wei, X. Zhou, Z. Xie, K. Li, Q. Ruan, C. Chen, J. Wang, C. A. Mirkin and Z. Zheng, *Small*, 2017, **13**, 1702003.

17 (*a*) V. Flauraud, M. Mastrangeli, G. D. Bernasconi, J. Butet, D. T. L. Alexander, E. Shahrabi, O. J. F. Martin and J. Brugger, *Nat. Nanotechnol.*, 2017, **12**, 73; (*b*) Y. Zhou,

X. Zhou, D. J. Park, K. Torabi, K. A. Brown, M. R. Jones, C. Zhang, G. C. Schatz and C. A. Mirkin, *Nano Lett.*, 2014, **14**, 2157; (*c*) W. Chen, M. Tymchenko, P. Gopalan, X. Ye, Y. Wu, M. Zhang, C. B. Murray, A. Alu and C. R. Kagan, *Nano Lett.*, 2015, **15**, 5254.

18 B. Yan, A. Thubagere, W. R. Premasiri, L. D. Ziegler, L. D. Negro and B. M. Reinhard, *ACS Nano*, 2009, **3**, 1190.

19 (*a*) D. Nepal, M. S. Onses, K. Park, M. Jespersen, C. J. Thode, P. F. Nealey and R. A. Vaia, *ACS Nano*, 2012, **6**, 5693; (*b*) L. C. Ma, R. Subramanian, H. W. Huang, V. Ray, C. U. Kim and S. J. Koh, *Nano Lett.*, 2007, **7**, 439.

20 (*a*) Q. Y. Lin, J. A. Mason, Z. Li, W. Zhou, M. N. O'Brien, K. A. Brown, M. R. Jones, S. Butun, B. Lee, V. P. Dravid, K. Aydin and C. A. Mirkin, *Science*, 2018, **359**, 669; (*b*) Q. Y. Lin, Z. Li, K. A. Brown, M. N. O'Brien, M. B. Ross, Y. Zhou, S. Butun, P. C. Chen, G. C. Schatz, V. P. Dravid, K. Aydin and C. A. Mirkin, *Nano Lett.*, 2015, **15**, 4699.

21 (*a*) M. Hajfathalian, K. D. Gilroy, S. D. Golze, A. Yaghoubzade, E. Menumerov, R. A. Hughes and S. Neretina, *ACS Nano*, 2016, **10**, 6354; (*b*) M. Hajfathalian, K. D. Gilroy, R. A. Hughes and S. Neretina, *Small*, 2016, **12**, 3444; (*c*) S. Neretina, R. A. Hughes, K. D. Gilroy and M. Hajfathalian, *Acc. Chem. Res.*, 2016, **49**, 2243.

22 (*a*) M. T. Perez Cardenas, C. Kong, J. He, S. Litvin, M. L. Meyerson and Z. Nie, *ACS Nano*, 2018, **12**, 1107; (*b*) K.-C. Kao, H. Nishi and T. Tatsuma, *Phys. Chem. Chem. Phys.*, 2018, **20**, 3735; (*c*) B. Sciacca, A. Berkhout, B. J. M. Brenny, S. Z. Oener, M. A. van Huis, A. Polman and E. C. Garnett, *Adv. Mater.*, 2017, **29**, 1701064; (*d*) A. A. El Mel, M. Chettab, E. Gautron, A. Chauvin, B. Humbert, J. Y. Mevellec, C. Delacote, D. Thiry, N. Stephant, J. Ding, K. Du, C. H. Choi and P. Y. Tessier, *J. Phys. Chem. C*, 2016, **120**, 17652; (*e*) G. Liu, C. Zhang, J. Wu and C. A. Mirkin, *ACS Nano*, 2015, **9**, 12137; (*f*) S. K. Cha, J. H. Mun, T. Chang, S. Y. Kim, J. Y. Kim, H. M. Jin, J. Y. Lee, J. Shin, K. H. Kim and S. O. Kim, *ACS Nano*, 2015, **9**, 5536.

23 C. V. Thompson, *Annu. Rev. Mater. Sci.*, 1990, **20**, 245.

24 P. Farzinpour, A. Sundar, K. D. Gilroy, Z. E. Eskin, R. A. Hughes and S. Neretina, *Nanoscale*, 2013, **5**, 1929.

25 K. D. Gilroy, A. Sundar, M. Hajfathalian, A. Yaghoubzade, T. Tan, D. Sil, E. Borguet, R. A. Hughes and S. Neretina, *Nanoscale*, 2015, **7**, 6827.

26 (*a*) K. D. Gilroy, A. Ruditskiy, H. Peng, D. Qin and Y. Xia, *Chem. Rev.*, 2016, **116**, 10414.

27 (*a*) Y. Le, Y. X. Yao and L. X. W. Lou, *Adv. Mater.*, 2018, 1800939; (*b*) X. Xia, Y. Wang, A. Ruditskiy and Y. Xia, *Adv. Mater.*, 2013, **25**, 6313.

28 Y. Sun, B. Wiley, Z. Y. Li and Y. Xia, *J. Am. Chem. Soc.*, 2004, 126, 9399.

29 (*a*) X. Wang, A. Ruditskiy and Y. Xia, *Natl. Sci. Rev.*, 2017, **3**, 520; (*b*) Z. Fang, Y. Wang, C. Liu, S. Chen, W. Sang, C. Wang and J. Zeng, *Small*, 2015, **11**, 2593.